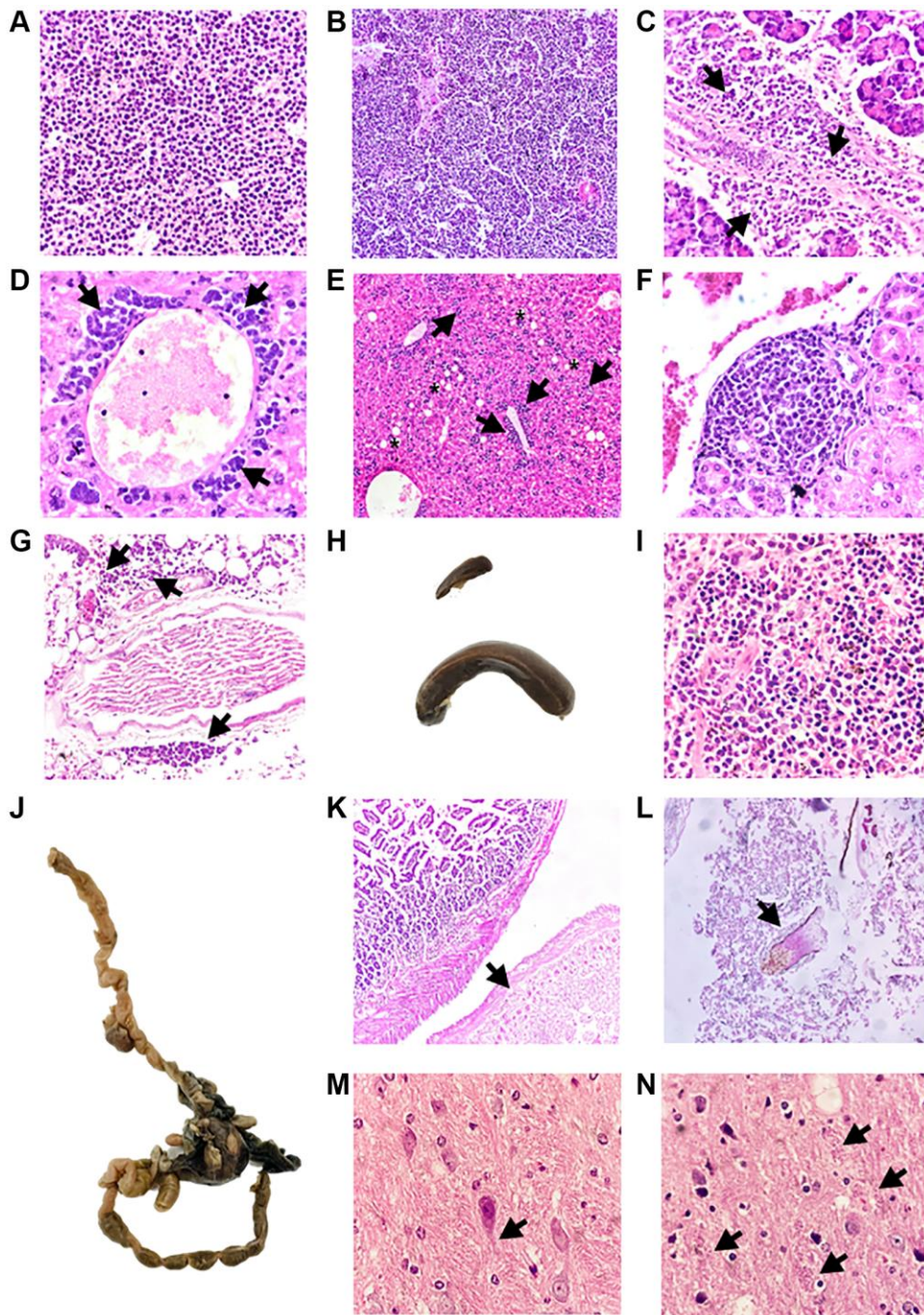
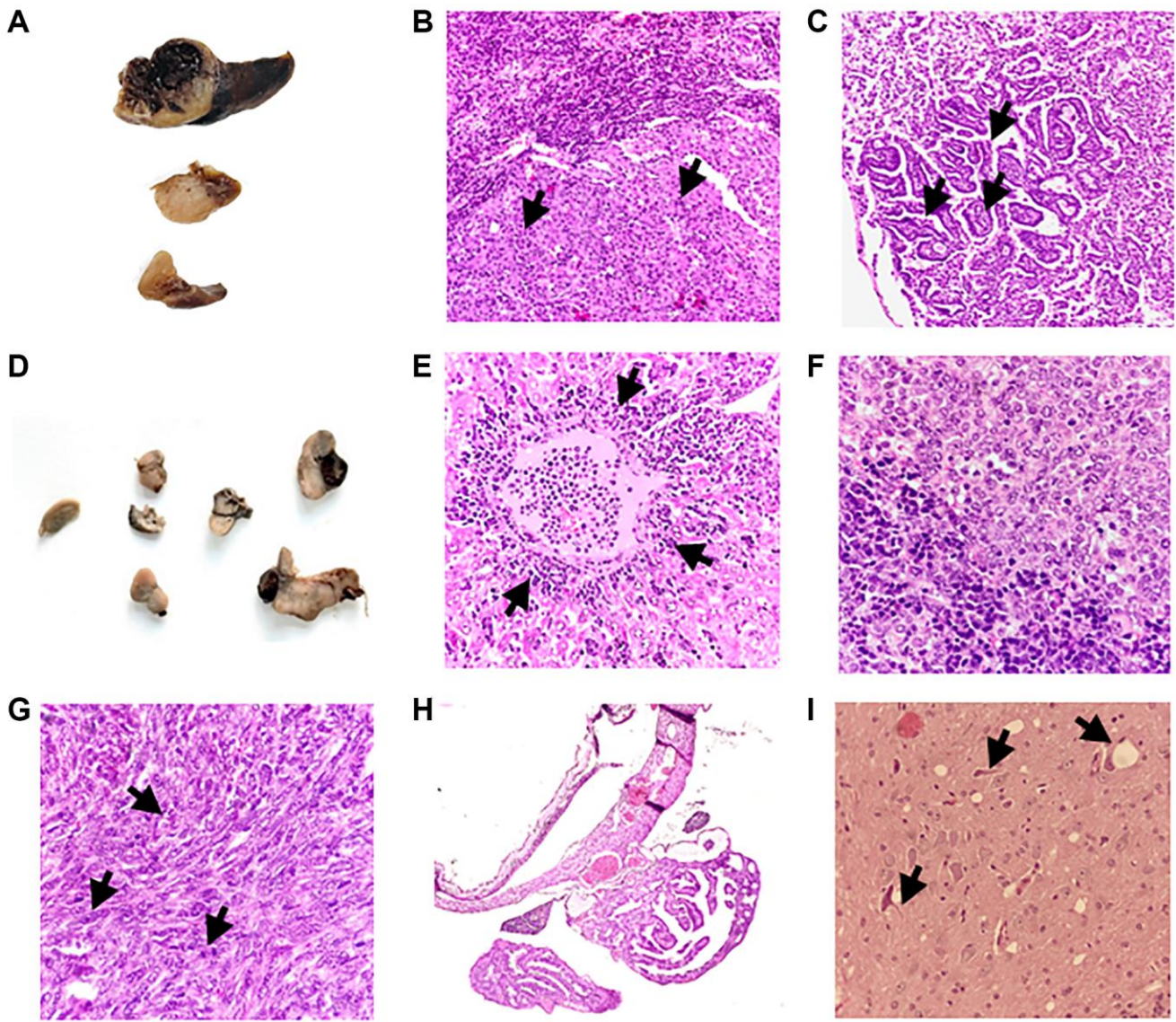


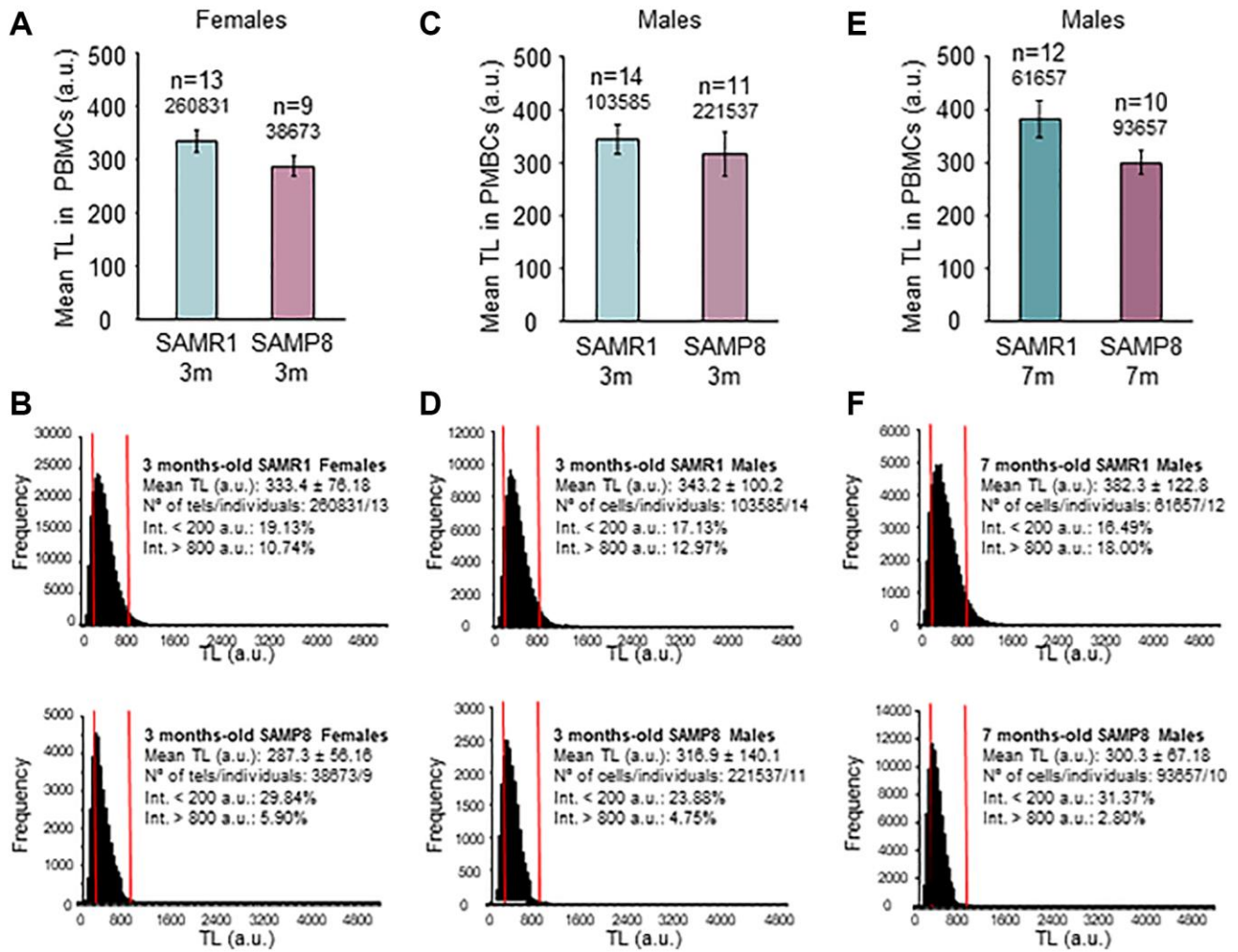
SUPPLEMENTARY FIGURES



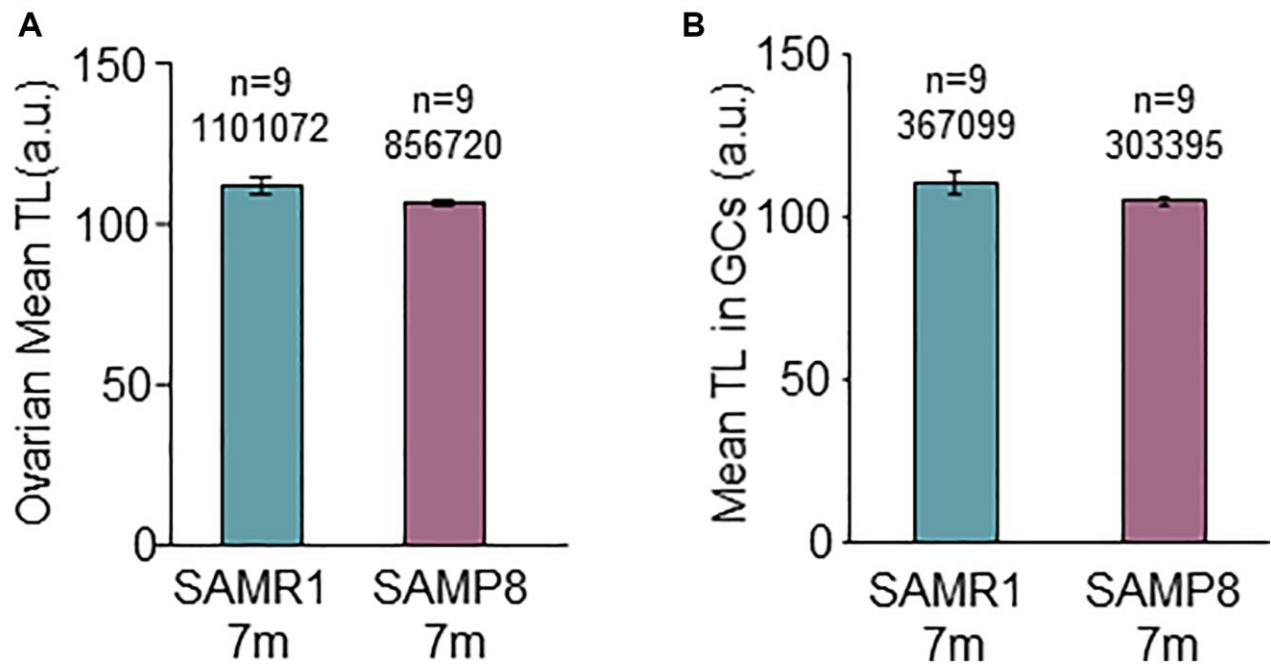
Supplementary Figure 1. Postmortem examinations of SAMP8 mice. Representative micrographs of necropsies in SAMP8. (A) Diffuse tumor infiltration of the thymus by lymphoid cells (SAMP8-18). (B) Lymphoid tumor with diffuse growth of cells of plasmablastic habitus in lymph node (SAMP8-07). (C) Lymphoid tumor lesions (indicated with arrows) in pancreatic tissue (SAMP8-07). (D) Lymphoid neoplasm infiltration (arrows) in hepatic perivenular areas (SAMP8-04). (E) Lymphoid tumor cellularity (plasmablastic, indicated with arrows) in hepatic sinusoids and perivenular areas (SAMP8-04). Asterisks indicate the presence of lipid droplets reflecting hepatic steatosis. (F) Lymphoid tumor lesions in kidney and (G) perirenal tissue (SAMP8-04). (H) Splenomegaly found in SAMP8 mice (SAMP8-07) (bottom) compared with a control spleen (top). (I) Diffuse splenic infiltration of lymphoma (SAMP8-18). (J) Intestinal torsion and necrosis (SAMP8-07). (K) Ischemic lesion (arrows) and (L) hairs (indicated with arrow) in feces in the intestine described in J. (M) Neurofibrillary tangles (indicated with arrows) in the brain (SAMPB-21). (N) Possible amyloid plaques (indicated with arrows) in brain (SAMP8-25).



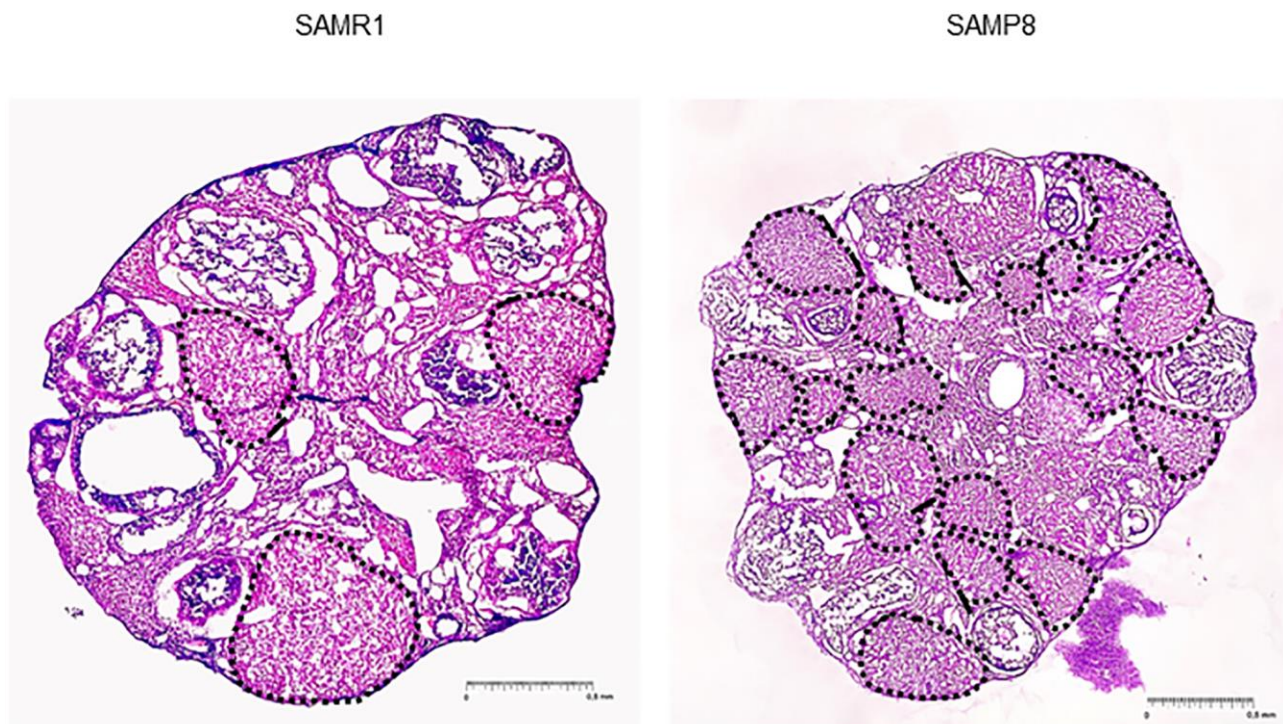
Supplementary Figure 2. Postmortem examinations of SAMR1 mice. Representative micrographs of necropsies in SAMR1. (A) Macroscopic image of a lung tumor (SAMR1-37). (B, C) Tumor foci in the lung consisting of papillary adenocarcinomas (SAMR1-37 in B and SAMR1-14 in C). Arrows indicate tumor areas. (D) Macroscopic image of lymph nodes thickened by tumors located adjacent to the colon, kidney and cervical region (SAMR1-07). (E) Metastasis of the lymphoma described in D in perivenular areas of liver, in the form of a small and large cell lymphoma (indicated by arrows). (F) Metastasis of the lymphoma described in D, infiltrated in spleen. Different cell morphologies are found. (G) Sarcoma in the abdominal wall (SAMR1 -25) consisting of a malignant spindle-cell lesion. Arrows indicate mitotic figures. (H) Image shows a benign cyst in peritoneum (SAMR1 -13). (I) Neurofibrillary tangles (indicated with arrows) in the brain (SAMR1 -25).



Supplementary Figure 3. Analysis of telomere length in PBMCs. (A) Mean TL of PBMCs, analyzed by HT-qFISH, in 3-month-old SAMP8 and SAMR1 females. (B) Telomere-length frequency histograms in 3-month-old SAMR1 (top panel) and SAMP8 females (lower panel). (C) Mean TL of PBMCs, analyzed by HT-qFISH, in 3-month-old SAMP8 and SAMR1 males. (D) Telomere-length frequency histograms in 3-month-old SAMR1 (top panel) and SAMP8 males (lower panel). (E) Mean TL of PBMCs, analyzed by HT-qFISH, in 7-month-old SAMP8 and SAMR1 males. (F) Telomere-length frequency histograms in 7-month-old SAMR1 (top panel) and SAMP8 males (lower panel). n indicates the number of mice analyzed. Underneath, the number of telomere spots analyzed is indicated. The S.E.M. is represented in error bars (A, C and E). Statistical significance was determined by unpaired *t*-test (A, C and E). *p*-values < 0.05 were considered statistically significant.



Supplementary Figure 4. Analysis of mean telomere length in the ovary. (A) Global mean TL in the ovary of 7-month-old SAMP8 and SAMR1 females, analyzed by FISH. (B) Mean TL in GCs of the ovary of mice described in A. n indicates the number of mice analyzed. Underneath, the number of telomere spots analyzed is indicated. The S.E.M. is represented in error bars, Statistical significance was determined by unpaired *t*-test (B) and Mann-Whitney *U* test (A). *p*-values < 0.05 were considered statistically significant.



Supplementary Figure 5. Corpus luteum in ovaries. Representative image of ovarian sections from SAMP8 (right panel) and SAMR1 (left panel) females. Dashed lines indicate corpus luteum.